International Journal of Technology 15(2) 342-352 (2024)
Received August 2023 / Revised September 2023 / Accepted September 2023

International Journal of Technology

http://ijtech.eng.ui.ac.id

Extraction and Characterization of Micro-fibrillated Cellulose from Rice Husk Waste for Biomedical Purposes

Nurhayati[1,2], Hari Eko Irianto[2], Rini Riastuti[1], Azizah Intan Pangesty[1,3], Adam F. Nugraha[1,4], Mitsugu Todo[5], Aidah Jumahat[6,7], Mochamad Chalid[1,4*]

[1]*Department of Metallurgical and Materials Engineering, Faculty of Engineering, Universitas Indonesia, Depok, 16424, Indonesia.*
[2]*Research Center for Marine and Land Bioindustry, National Research and Innovation Agency, Lombok 83352, Indonesia.*
[3]*Research Center for Biomedical Engineering, Faculty of Engineering, Universitas Indonesia, Depok 16424, Indonesia.*
[4]*Center for Sustainability and Waste Management, Universitas Indonesia, Depok, 16424, Indonesia.*
[5]*Research Institute for Applied Mechanics, Kyushu University, Kasuga-koen 6-1, Kasuga-shi, Fukuoka 816-8580, Japan.*
[6]*Faculty of Mechanical Engineering, Universiti Teknologi MARA, Shah Alam 40450, Malaysia.*
[7]*Institute for Infrastructure Engineering Sustainable and Management, Universiti Teknologi MARA, Shah Alam 40450, Malaysia.*

Abstract. This study aimed to report the extraction of micro-fibrillated cellulose (MFC) from rice husk (RH) through a series of processes including alkalization, bleaching, chemical hydrolysis, and mechanical treatment. The chemical structure, morphology, and crystallinity were assessed using Fourier Transform Infrared spectroscopy (FTIR), Scanning Electron Microscope (SEM), and X-ray diffraction (XRD). The results showed that alkalization was more effective in removing unwanted substances such as silica, hemicellulose, and lignin compared to bleaching. Chemical or mechanical treatment was more targeted towards removing the amorphous phase while fibrillating MFC. Further mechanical treatment significantly enhanced the crystallinity index (CI) of MFC, reaching 87.47%, while chemical treatment remained at 78.54%. The mechanical treatment led to a larger void size due to rigorous fibrillation, resulting in increased water retention during extraction compared to chemically treated MFC with a negatively charged surface. Crystal extraction through mechanical treatment disrupted the hydrogen bond, transforming cellulose crystal from triclinic Iα to monoclinic Iβ. The comprehensive evaluation of MFC extracted from RH showed its potential for biomedical application.

Keywords: Acid hydrolysis; Mechanical treatment; Micro-fibrillated cellulose; Rice husk

1. Introduction

Exploration of bio-based materials is a process for addressing global challenges such as the lack of petroleum, climate change, and unmanageable waste. Cellulose, a member of the polysaccharide family, is the most prevalent organic component generated from biomass. This material has diverse applications in industries, including textiles (Felgueiras

*Corresponding author's email: m.chalid@ui.ac.id, Tel.: +62-21-786-3510; Fax.: +62-21-787-2350
doi: 10.14716/ijtech.v15i2.6698

et al., 2021), food (Suryanti *et al.,* 2023; Mu *et al.*, 2019), and filtration membranes (Rochardjo, Fatkhurrohman, and Yudhanto, 2021). Cellulose holds tremendous potential as a biomedical material due to its biocompatibility, biodegradability, water-retention capacity, renewability, and tunability, making it an ideal biopolymer (Hu *et al.,* 2021; Iwamoto, Nakagaito, and Yano, 2007). Micro-fibrillated cellulose (MFC) offers advantages as a pharmaceutical excipient for extended and controlled drug release, as well as reinforcing hydrogels and composites in biomaterial implants (Pandey 2021).

The use of environmentally friendly and sustainable biomedical materials has become increasingly important in healthcare studies and development. Rice husk (RH) waste, the outer covering of rice grains resulting from the milling process, constitutes a natural fiber comprising cellulose, hemicellulose, lignin, and other compounds such as wax, pectin, and silica (Johar, Ahmad, and Dufresne, 2012). Studies showed that RH contained cellulose (25-35%), lignin (26-31%), hemicellulose (18-21%), and silica (15-17%) (Rezanezhad, Nazarnezhad, and Asadpour, 2013).

An extensive study has been conducted on the isolation of cellulose from biomass/natural fibers. This process aimed to remove lignin, hemicellulose, and other non-cellulose compounds that naturally encapsulate cellulose. Alkalization and bleaching are the most commonly used chemical treatments. These treatments not only remove non-cellulose components but also defibrillate cellulose fibers into micro-sized (Yuanita *et al.,* 2015). Menawhile, mechanical treatment through grinding is a straightforward, energy-efficient process that requires simple equipment. Uetani and Yano (2011) explored the isolation of nano-fibrillated cellulose using a modified blender. In the mechanical grinding method, shear forces from the blades break hydrogen bonds, reducing cellulose cell wall size to the nanoscale (Abdul-Khalil *et al.,* 2014). Therefore, this study aimed to compare the effect of chemical and mechanical treatments on the characteristics of micro/nano-fibrillated cellulose as a biomedical material. The resulting material from processed RH holds potential applications in various medical fields, including surgical paper, wound coverings, bone patch devices, and drug delivery systems.

2. Methods

2.1. Materials

RH (Oryza sativa L.) was obtained from a local rice field in Wonogiri, Central Java, Indonesia. Sodium hydroxide (NaOH, 99.9%), Sodium chlorite ($NaClO_2$, 25%), and acetic acid (CH_3COOH, 99%) were procured from Merck, while sulfuric acid (H_2SO_4, 96.1%) was obtained from Mallinckrodt AR.

2.2. Treatment Preparation

In this study, virgin RH was subjected to sequential treatments by alkalization, bleaching, and hydrolysis or mechanical methods, to obtain the treated RH as RH_Al, RH_Al-Bl, and RH_Al-Bl-Ch or RH_Al-Bl-Mc, respectively. The following section provides the details for each process.

2.2.1. Pre-treatment

MFC extraction from RH comprised 2 primary steps, namely pretreatment (washing, crushing, alkalization) and MFC isolation using either mechanical or chemical methods. Pre-treatment began with washing RH fibers in flowing water to remove visible debris, followed by soaking RH and drying it at room temperature for 24 hours. The soaked fibers were then crushed through a 40-mesh sieve and alkalinized in a 5 w/w% NaOH solution at a 1:25 w/v ratio for 2 hours while stirring at approximately 80°C. After draining and rinsing with distilled water, alkalized RH fibers were bleached for 2 hours at 70°C using 1.7% $NaClO_2$ in

a buffer of 100 ml of 0.2 M acetic acid and 0.291 g NaOH. According to Iwamoto, Nakagaito, and Yano (2007), this bleaching process was repeated 5 times until the sample was cloudy white. Finally, the obtained product was rinsed with distilled water to remove residual lignin, hemicellulose, and chlorine ions. Observations were conducted at each step, including RH, fibers after alkaline treatment (RH_Al), as well as fibers after alkaline and bleaching treatments (RH_Al-Bl).

2.2.2. MFC Isolation

Following the removal of lignin, hemicellulose, and other impurities, the pre-treatment was followed by isolating MFC through acid hydrolysis (RH_Al-Bl-Ch) and mechanical milling, (RH_Al-Bl-Mc). In this study, MFC results from both methods were compared to identify the most effective. Acid hydrolysis treatment was performed by adding 60% v/v sulfuric acid to the pre-treated RH fibers in distilled water (1/25 of w/v) and mixing at 45°C (Syafri *et al.* 2011). After 45 minutes, the hydrolysis was terminated by adding cold distilled water (about 15°C). For the mechanical milling treatment, water (98/2 of w/w) was added to the pre-treated RH fibers in a blender, and the blade was rotated between 11,000 - 12,000 rpm at room temperature for 20 minutes (Johar, Ahmad, and Dufresne, 2012).

2.2.3. Characterizations

RH at each treatment stage was evaluated by using a Field Emission Scanning Electron Microscopes (FE-SEM) Quanta 650 EDAX EDS Analyzer at varying magnifications of 100 and 500 times. Crystallinity percentage was determined through hydrogen bonding analysis, using FTIR spectroscopy (Perkin Elmer 90325) and X-ray diffraction (XRD) with a Philips XRD. FTIR was also adopted to investigate the chemical structure, while XRD data was analyzed to assess polymorphism and the allomorph of the extracted MFC. The crystallinity ratio (CrR) and hydrogen bond energy (EH) for specific OH stretching bands in cellulose fibers were calculated by comparing absorbance peaks at 1372 cm^{-1} (A1372) and 2900 cm^{-1} (A2900) (Nelson and O'Connor 1964). Gaussian deconvolution peak separation methods were applied to XRD data to obtain the crystallinity index (CI) of cellulose fibers, calculated using the Segal Equation (Park *et al.*, 2010).

3. Results and Discussion

3.1. Physical Appearance

This study adopted alkalization, bleaching, hydrolysis, and mechanical treatment methods to extract MFC and separate it from unwanted impurities. These methods yielded distinct physical changes, particularly in color and texture.

Figure 1 Physical appearance of isolated husk rice fibers for (a) RH, (b) RH_Al, and (c) RH_Al-Bl

Figure 1 shows the significant morphological changes observed during MFC isolation process. A noticeable color shift was discovered in each phase, showing a reduction in impurities such as lignin, hemicellulose, and silica, hemicellulose, and silica. RH_Al sample maintained a dark color compared to RH, suggesting the presence of lingering lignin. In

contrast, RH_Al-Bl sample was white, showing the effective removal of lignin during the bleaching steps.

3.2. Morphology Evolution

Figure 2a–e shows the SEM images at 100 and 500× magnification for each sample. MFC isolation process comprised unfolding from the sheet into separate fibrils, resulting in a reduction in fibril width and the formation of a network structure. In Figure 2a, SEM image of the as-received RH sample lemma surface showed papillae (Park *et al.,* 2003) and hairs of various sizes (Chen, Xu, and Shivkumar, 2018). However, several areas that lack these structures, disintegrated during rice milling. The outer epidermis had an uneven linear furrow decorated with conical protrusions, each comprising plant cell walls with bundled cellulose and lignin. Silica, an impurity, was concentrated at the tip and shoulders of these protrusions (Chen, Xu, and Shivkumar, 2018). Figure 2b shows the retainment of ridged structures with furrows, indicating multiple layers of cell walls (Ludueña *et al.,* 2011). Furthermore, the protrusions and hairs were removed, showing partial hemicellulose and lignin removal. Silica was visibly reduced, exposing the inner "cat-eyes" structure of the epidermis. Based on Figure 2c, after bleaching, large sheets were absent, and fibrils were visible. Some remnants of large sheets suggest lingering lignin, supported by FTIR. Additionally, segments of fibril sheets implied MFC network agglomeration (Choi *et al.,* 2019).

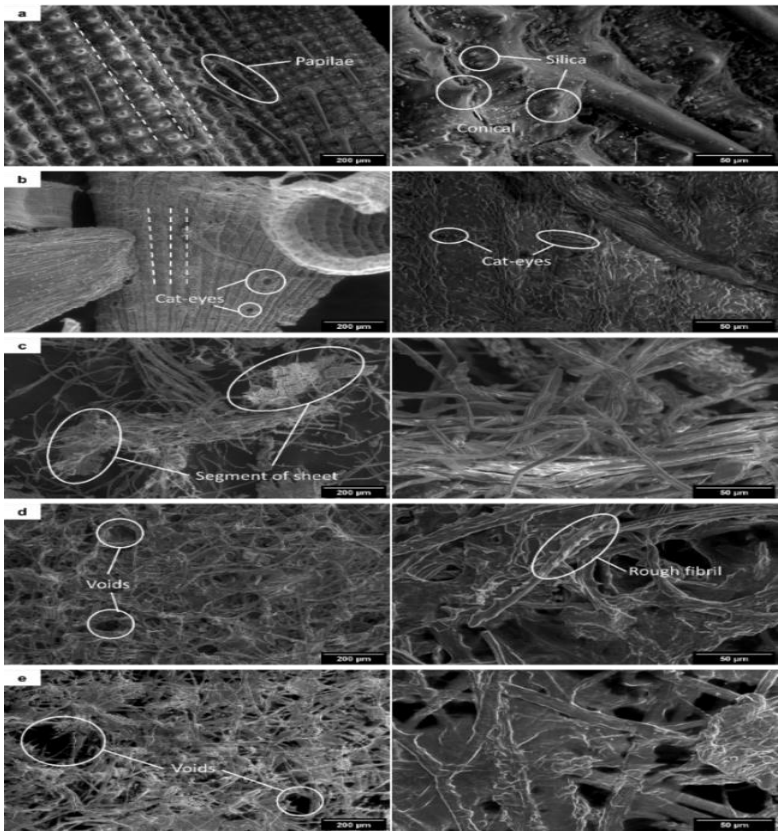

Figure 2 SEM images with 100x (left) and 500x (right) magnification of each sample; (a) RH, (b) RH_Al (c) RH_Al-Bl (d) RH_Al-Bl-Ch, (e) RH_Al-Bl-Mc

Figures 2d (chemical) and 2e (mechanical) showed that surface patterns, namely RH_Al-Bl-Ch had spiky surfaces, while RH_Al-Bl-Mc was smoother (Galera Manzano *et al.,* 2021). These methods aimed to remove cellulose amorphous phase, thereby enhancing water vapor retention and exposing hydroxyl and carboxyl groups. Sulfuric acid hydrolysis, particularly in the amorphous phase lacking protective steric hindrance in the crystalline

region, results in half-ester sulfate groups on cellulose surface, generating a highly negative charge (Rajinipriya *et al.,* 2018). Achieved either chemically or mechanically, cellulose fibrillation divides MFC into smaller fibrils, exposing hydroxyl and carboxyl groups and enhancing water vapor retention in both samples (Väisänen *et al.*, 2018).

3.3. Chemical Structure Analysis

The chemical structure of the samples was observed through FTIR spectra (Figure 3a). The peak at approximately 1555 cm^{-1}, attributed to lignin according to Wyman *et al.* (2004), diminished as expected in RH_Al sample compared to RH, and it became broader and disappeared in samples RH_Al-Bl.

A similar pattern was observed for the slight bump around 800 cm^{-1}, showing silica in RH samples, which was removed in RH_Al, RH_Al-Bl, and RH_Al-Bl-Ch or RH_Al-Bl-Mc. The valley of 1260 cm^{-1} in FTIR signal, represented another impurity, such as hemicellulose, coexisting with the prominent cellulose peak at 1300 cm^{-1}. This valley weakened and split from RH_Al to further treated samples, signifying the effective removal of silica during the initial alkalization.

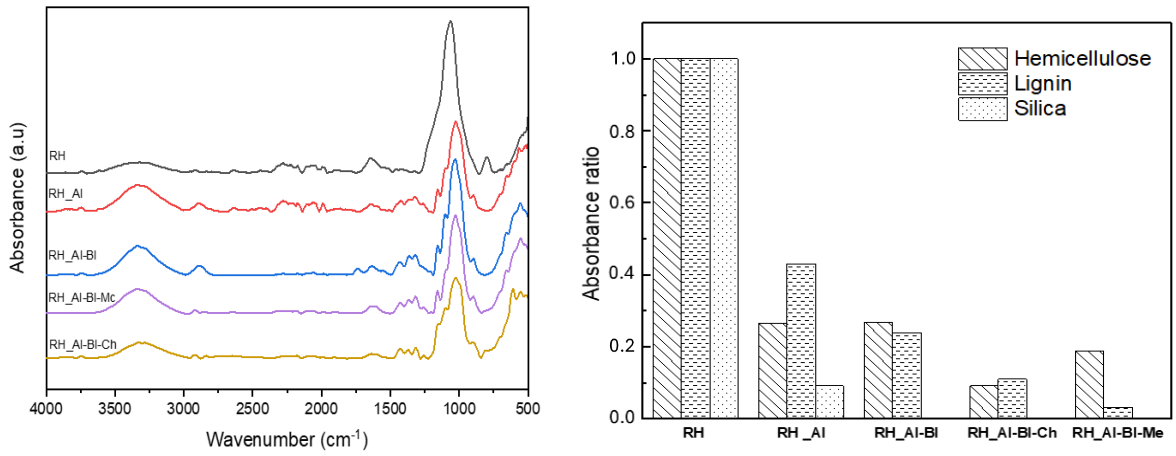

Figure 3 a) FTIR spectra absorbance; b) Absorbance ratio of hemicellulose, lignin, silica.

Figure 3b compiles the impurity content in the RH sample, using absorbance ratios to provide a detailed assessment of impurities. The ratios at 800 cm^{-1}, 1260 cm^{-1}, and 1555 cm^{-1} represent silica, hemicellulose, and lignin, respectively, with the as-received RH sample serving as the reference. Figure 3b shows a significant reduction in all impurities, at least 45%, starting from alkalization treatment. Alkalization substantially reduced silica content, with the entire elimination being performed through bleaching. Hemicellulose and lignin ratios also decreased after alkalization and further decreased due to mechanical or chemical treatment.

Chemical or mechanical treatments were applied to further reduce impurities and extract MFC. The primary objective is to remove the amorphous region and unbundle micro and nanofibrils of cellulose network using different strategies. Chemical treatment uses sulfuric acid, following the same principle as alkalization, to isolate and fibrillate cellulose by hydrolyzing the glucoside bonds in lignin and hemicellulose chains (Jamalpoor and Hosseini 2015).

3.4. Crystallinity Behavior

3.4.1. Hidrogen bond energy (EH) and bond distance (R)

In discussing sample crystallization behavior, FTIR absorption peaks in the 1700-850 cm^{-1} range aid in assessing cellulose polymorphism. A shift in C-C and C-O vibration peaks

showed the conversion of cellulose allomorph from type I to II. According to Carrillo *et al.* (2004), when cellulose type I is more dominant than type II, the absorption at 1420 and 1155 cm^{-1} would change to approximately 1430 and 1162 cm^{-1}, respectively. Therefore, the absorption at approximately 1430 and 1162 cm^{-1} in all sample spectra showed the presence of cellulose I.

Absorption at 893 cm^{-1} for cellulose type I changed to approximately 897 cm^{-1}. The 895-905 cm^{-1} range was in line with higher wavenumbers indicating cellulose type I, consistent with Yue (2011), and attributed to glucose residue rotation around the glycosidic bond (Jamalpoor and Hosseini 2015). Furthermore, all fibers had an absorption peak at 1315 cm^{-1}, confirming the minor presence of cellulose type II. FTIR analysis reinforces cellulose I dominance in both untreated and treated RH samples.

EH and R analysis offered another method to distinguish cellulose types. Cellulose type I had 3 hydrogen bonding arrangements, namely intramolecular hydrogen bonds O(6)H···O(2) and O(3)H···O(5), as well as intermolecular hydrogen bond O(6)H···O'(3) with FTIR absorption peaks around 3455-3410 cm^{-1}, 3375-3340 cm^{-1}, and 3310-3230 cm^{-1}, respectively. Meanwhile, cellulose type II had 4 hydrogen bond arrangement, similar to type I, with the addition of an intermolecular hydrogen bond: O(2)H···O'(2) or O(6)H···O'(3) (Poletto *et al.,* 2011). Table 1 provides EH and R values for each sample. Compared to EH value of the as-received RH, all treated samples had lower hydrogen bond energy, consistent with Poletto *et al.,* (2011).

Table 1 Values of EH and R for each sample

Sample Name	Intramolecular O(2)H···O(6) 3460-3405 cm^{-1}		Intramolecular O(3)H···O(5) 3375-3340 cm^{-1}		Intermolecular O(2)H···O'(2) 3310-3230 cm^{-1}	
	EH (kJ/mol)	R (Å)	EH (kJ/mol)	R (Å)	EH (kJ/mol)	R (Å)
RH	17.692	2.796	24.452	2.775	28.839	2.761
RH_Al	18.483	2.793	23.229	2.778	30.134	2.757
RH_Al-Bl	15.750	2.802	23.158	2.779	30.565	2.755
RH_Al-Bl-Ch	15.750	2.802	23.229	2.778	26.394	2.768
RH_Al-Bl-Mc	11.651	2.815	20.856	2.786	28.911	2.761

The relative hydrogen bond distances examined in this study range from 2.755 to 2.815 Å. According to Tasker *et al.*, the hydrogen bond distance of Cellulose I was 2.75 Å. Consequently, the proximity of the distance to this value showed the refinement of cellulose in the sample (O'Sullivan 1997). Additionally, as stated by Poletto *et al.,* (2011), higher crystallinity leads to denser cellulose packing and shorter distances, resulting in increased hydrogen energy between cellulose molecules.

Nelson and O'Connor (1964) proposed the ratio between FTIR absorbance bands at 1372 and 2900 cm^{-1} as CrR, which is proportional to the crystallinity degree of cellulose. CrR values for RH, RH_Al, RH_Al-Bl, RH_Al-Bl-Ch, and RH_Al-Bl-Mc were 0.79, 1.73, 2.17, 3.03, and 5.67, respectively. The values gradually increase along with the treatment process, with RH_Al-Bl-Mc having the highest. This suggested that mechanical treatment was more powerful compared to chemical treatment in removing the amorphous region.

3.4.2. Crystallinity Index (CI)

XRD was used to complement the other characterization and further evaluate the crystallinity behavior of cellulose. Figure 8 shows XRD diffraction of untreated and treated RH. From XRD diffraction data, several peaks were identified, where peak one at 2θ=14.5° is Iα (100) and Iβ (10), peak two at 2θ=17.0° is Iα (010) and Iβ (110), peak three at 2θ=22.5° is Iα ($\overline{1}12$) or (002) and Iβ (012), as well as peak four at 2θ=34.0° is Iα ($\overline{1}14$) and Iβ (004)

(Hult *et al.,* 2003; Wada and Okano, 2001). XRD peaks were processed by Gaussian deconvolution separation to further determine the crystallinity index, the d-spacing, crystallite size, and Z-values.

In this study, Z-values function developed by Wada and Okano (2001) was used to determine cellulose crystal structure, identifying it as either triclinic (Iα) or monoclinic (Iβ) allomorph. The most intense crystalline peak was discovered at 22.62° on the (002) lattice plane for all the samples. Lionetto *et al.* and Harahap *et al.* investigations also identified the same peak within different scanning angles (2θ) (Harahap *et al.,* 2023; Lionetto *et al.,* 2012).

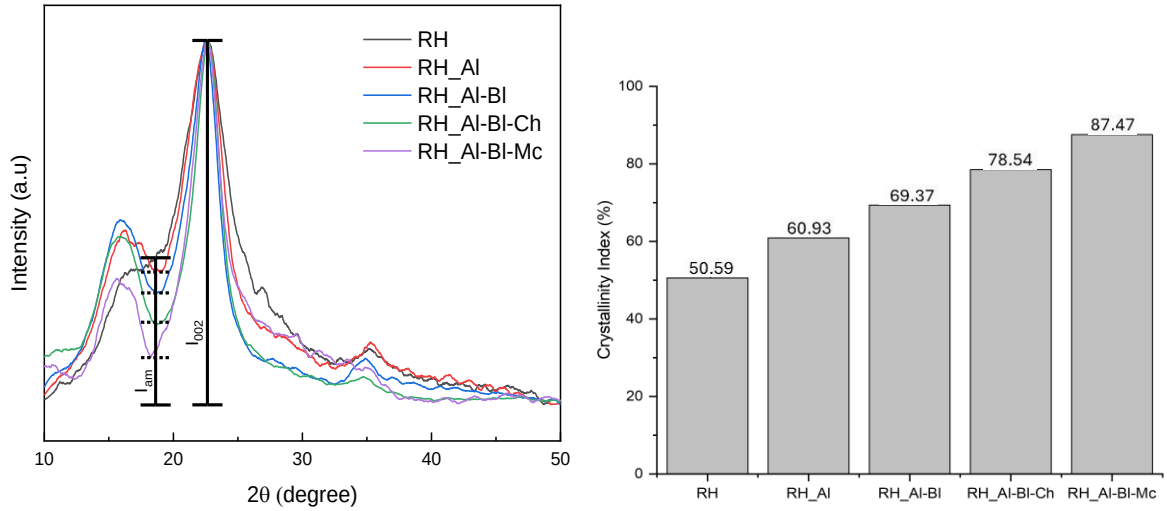

Figure 4 a) XRD spectra; b) CI for each sample

Figure 4a shows a decreasing amorphous trench between peak (002) and peak (010) during each treatment phase, moving towards the baseline, while CI is reversely increasing. Quantitatively, Figure 4b showed a continuous rise in CI in the treatment process, with mechanical treatment showing superiority compared to the chemical counterpart. CI of MFC shows a tightly packed structure, hypothetically improving thermal stability and mechanical properties, making it desirable for composite applications (Poletto *et al.,* 2011).

Table 2 Crystallite size (L) from each sample

Sample Name	*L* (110) (nm)	*L* ($1\bar{1}0$) (nm)	*L* (002) (nm)	*L* (004) (nm)	*L* (100) (nm)	*L* (010) (nm)	*L* (110) (nm)	*L* ($\bar{1}\bar{1}4$) (nm)
RH	6.91	2.33	1.79	7.99				
RH_Al	5.73	2.27	1.51	8.83				
RH_Al-Bl	5.65	2.21	6.74	10.13				
RH_Al-Bl-Ch	6.36	1.01	7.52	5.28				
RH_Al-Bl-Mc					6.97	0.67	5.77	3.03

The crystallite size of the samples decreases during the treatment process, as shown in Table 2. When cellulose fiber was more distanced, smaller crystal sizes were observed, often associated with a change in crystal structure. The desirable triclinic structure of crystal Iα in RH for MFC isolation is prone to hydrogen bonding breakdown. However, when the triclinic structure loses integrity, it will rearrange to create a monoclinic structure of Iβ. This suggested that the final mechanical treatment entirely transformed cellulose crystal from Iα to I*β*. The transformation was also shown in Table 2, where the crystallographic family was diverted from triclinic structure (110); ($1\bar{1}0$); (002); (004); (100) to monoclinic structure (010); (110); ($\bar{1}\bar{1}4$).

3.5. Biomedical Potential

This study presents the potential of MFC extracted from RH as a biomedical material for innovative applications (Varshney *et al.,* 2022). The successful removal of unwanted substances such as silica, hemicellulose, and lignin through alkalization and bleaching treatments showed the suitability for medical applications where purity and biocompatibility were crucial (Islam *et al.,* 2018). The pristine MFC structure achieved through these processes presents a clean surface, minimizing adverse reactions when interacting with biological systems (Sunasee, Hemraz, and Ckless, 2016). Finally, the impurity-free nature of MFC positions it as a promising candidate for wound healing and tissue engineering, where seamless integration with the natural processes of the body is essential.

The substantial increase in CI of MFC due to rigorous mechanical treatment is essential with potential biomedical implications. This heightened CI signifies a more ordered and aligned cellulose structure, enhancing mechanical strength and stability, particularly beneficial for regenerative medicine scaffolds (Mauck and Burdick, 2015). The unique voids observed in mechanically treated MFC, showing increased water retention, offered opportunities for controlled drug delivery systems. These interconnected voids serve as therapeutic agent reservoirs. This controlled release mechanism holds promise for precise and sustained pharmaceutical delivery to enhance patient outcomes (Sun *et al.,* 2019). Further mechanical processes elevate CI of MFC to 87.47%. This improved mechanical strength and stability, crucial for biomedical applications (Seddiqi *et al.,* 2021). Mechanically treated negatively charged surfaces aid interactions with positively charged cells and medical materials, supporting its usage in wound healing and as a medical adhesive. Additionally, mechanical treatment shifts cellulose crystal structure from triclinic Iα to monoclinic Iβ, while reducing MFC crystallite size, potentially affecting mechanical properties and reactivity.

4. Conclusions

In conclusion, this study delved into the evolution of MFC crystallinity through a multi-stage extraction process, comprising alkalization, bleaching, and either chemical or mechanical treatment. Alkalization proved effective in removing silica and hemicellulose from RH while bleaching primarily eliminated the bulky lignin structure. These procedures not only heightened MFC purity, assessed both visually and chemically using FTIR, but also improved crystallinity, scrutinized through XRD. Successful efforts were made to eliminate the amorphous phase through both chemical and mechanical treatments, substantiated by SEM images showcasing fibrillation. This fibrillation was accompanied by a decrease in EH, an increase in R, and a slight reduction in crystallite size and width. Smaller MFC widths resulting from mechanical treatment led to higher surface energy, rendering the surface more water-attractive. Furthermore, cellulose crystals in MFC, extracted using both methods, predominantly had cellulose Iα, transitioning to Iβ, specifically pronounced after mechanical treatment due to hydrogen bond rearrangement. These discoveries firmly established MFC as a highly promising biomedical material with versatile potential across various medical applications.

Acknowledgments

This research was funded by Universitas Indonesia with grant number NKB-678/UN2.RST/HKP.05.00/2021. The authors are grateful to Aldhi Saputro for the laboratory activity.

References

Abdul-Khalil, H.P.S., Davoudpour, Y., Islam, M.N., Mustapha, A., Sudesh, K., Dungani, R., Jawaid, M., 2014. Production and Modification of Nanofibrillated Cellulose Using Various Mechanical Processes: A Review. *Carbohydrate Polymers*, Volume 99, pp. 649–665

Carrillo, F., Colom, X., Suñol, J.J., Saurina, J., 2004. Structural FTIR analysis and thermal characterization of lyocell and viscose-type fibers. European Polymer Journal, Volume 40(9), pp. 2229–2234

Chen, Z., Xu, Y., Shivkumar, S., 2018. Microstructure and Tensile Properties of Various Varieties of Rice Husk. *Journal of the Science of Food and Agriculture*, Volume 98(3), pp. 1061–1070

Choi, K., Nam, J.D., Kwon, S.H., Choi, H.J., Islam, M.S., Kao, N., 2019. Microfibrillated Cellulose Suspension and its Electrorheology. *Polymers,* Volume 11(12), p. 2119

Felgueiras, C., Azoia, N.G., Gonçalves, C., Gama, M., Dourado, F., 2021. Trends on the Cellulose-Based Textiles: Raw Materials and Technologies. Frontiers in Bioengineering and Biotechnology, Volume 9, p. 608826

Galera-Manzano, L.M., Ruz Cruz, M.Á., Moo Tun, N.M., Valadez González, A., Mina Hernandez, J.H., 2021. Effect of Cellulose and Cellulose Nanocrystal Contents on the Biodegradation, Under Composting Conditions, of Hierarchical Pla Biocomposites. *Polymers*, Volume 13(11), p. 1855

Harahap, M., Daulay, N., Zebua, D., Gea, S., 2023. Nanofiber Cellulose/Lignin from Oil Palm Empty Fruit Bunches and the Potential for Carbon Fiber Precursor Prepared by Wet-spinning. *International Journal of Technology*, Volume 14(1), pp. 152–161

Hu, L., Zhong, Y., Wu, S., Wei, P., Huang, J., Xu, D., Zhang, L., Ye, Q., Cai, J., 2021. Biocompatible and Biodegradable Super-toughness Regenerated Cellulose via Water Molecule-assisted Molding. *Chemical Engineering Journal*, Volume 417, p. 129229

Hult, E.L., Iversen, T., Sugiyama, J., 2003. Characterization of the Supermolecular Structure of Cellulose in Wood Pulp Fibers. *Cellulose,* Volume 10(2), pp. 103–110

Islam, M.S., Kao, N., Bhattacharya, S.N., Gupta, R., Choi, H.J., 2018. Potential Aspect of Rice Husk Biomass in Australia for Nanocrystalline Cellulose Production. *Chinese Journal of Chemical Engineering*, Volume 26(3), pp. 465–476

Iwamoto, S., Nakagaito, A.N., Yano, H., 2007. Nano-fibrillation of Pulp Fibers for the Processing of Transparent Nanocomposites. *Applied Physics A: Materials Science and Processing,* Volume 89(2), pp. 461–466

Jamalpoor, A., Hosseini, M., 2015. Biaxial Buckling Analysis of Double-orthotropic Microplate-systems Including in-plane Magnetic Field Based on strain gradient theory. *Composites Part B: Engineering,* Volume 75, pp. 53–64

Johar, N., Ahmad, I., Dufresne, A., 2012. Extraction, preparation, and characterization of cellulose fibers and nanocrystals from rice husk. *Industrial Crops and Products,* Volume 37(1), pp. 93–99

Lionetto, F., Del-Sole, R., Cannoletta, D., Vasapollo, G., Maffezzoli, A., 2012. Monitoring wood degradation during weathering by cellulose crystallinity. *Materials,* Volume 5(10), pp. 1910–1922

Ludueña, L., Fasce, D., Alvarez, V.A., Stefani, P.M., 2011. Nanocellulose from Rice Husk Following Alkaline Treatment to Remove Silica. *BioResources*, Volume 6(2)

Mauck, R.L., Burdick, J.A., 2015. From Repair to Regeneration: Biomaterials to Reprogram the Meniscus Wound Microenvironment. *Annals of Biomedical Engineering*, Volume 43(3), pp. 529–542

Mu, R., Hong, X., Ni, Y., Li, Y., Pang, J., Wang, Q., Xiao, J., Zheng, Y., 2019. Recent Trends and Applications of Cellulose Nanocrystals in Food Industry. *Trends in Food Science and Technology*, Volume 93, pp. 136–144

Nelson, M.L., O'Connor, R.T., 1964. Relation of Certain Infrared Bands to Cellulose Crystallinity and Crystal Lattice Type. Part II. A New Infrared Ratio for Estimation of Crystallinity in Celluloses I and II. *Journal of Applied Polymer Science,* Volume 8(3) , pp. 1325–1341

O'Sullivan, A.C., 1997. Cellulose: The Structure Slowly Unravels. *Cellulose*, Volume 4(3), pp. 173–207

Pandey, A. 2021. Pharmaceutical and Biomedical Applications of Cellulose Nanofibers: a Review. *Environmental Chemistry Letters*, Volume 19(3), pp. 2043–2055

Park, B.D., Gon Wi, S., Ho Lee, K., Singh, A.P., Yoon, T.H., Soo-Kim, Y., 2003. Characterization of Anatomical Features and Silica Distribution in Rice Husk using Microscopic and Micro-analytical Techniques. *Biomass and Bioenergy*, Volume 25(3), pp. 319–327

Park, S., Baker, J.O., Himmel, M.E., Parilla, P.A., Johnson, D.K., 2010. Cellulose Crystallinity Index: Measurement Techniques and Their Impact on Interpreting Cellulase Performance. *Biotechnology for Biofuels*, Volume 3, pp. 1–10

Poletto, M., Pistor, V., Zeni, M., Zattera, A.J., 2011. Crystalline Properties and Decomposition Kinetics of Cellulose Fibers in Wood Pulp Obtained by Two Pulping Processes. *Polymer Degradation and Stability*, Volume 96(4), pp. 679–685

Rajinipriya, M., Nagalakshmaiah, M., Robert, M., Elkoun, S., 2018. Importance of Agricultural and Industrial Waste in the Field of Nanocellulose and Recent Industrial Developments of Wood Based Nanocellulose: A Review. American Chemical Society (*ACS) Sustainable Chemistry and Engineering*, Volume 6(3), pp. 2807–2828

Rezanezhad, S., Nazarnezhad, N., Asadpour, G., 2013. Isolation of Nanocellulose from Rice Waste via Ultrasonication. *Lignocellulose*, Volume 2(1), pp. 282–291

Rochardjo, H.S.B., Fatkhurrohman, AK., Yudhanto, F., 2021. Fabrication of Nanofiltration Membrane Based on Polyvinyl Alcohol Nanofibers Reinforced with Cellulose Nanocrystal using Electrospinning Techniques. *International Journal of Technology*, Volume 12(2), pp. 329–338

Seddiqi, H., Oliaei, E., Honarkar, H., Jin, J., Geonzon, L.C., Bacabac, R.G., Klein-Nulend, J., 2021. Cellulose and its Derivatives: Towards Biomedical Applications. *Cellulose*, Volume 28(4), pp. 1893–1931

Sun, B., Zhang, M., Shen, J., He, Z., Fatehi, P., Ni, Y., 2019. Applications of Cellulose-based Materials in Sustained Drug Delivery Systems. *Current Medicinal Chemistry*, Volume 26(14), pp. 2485–2501

Sunasee, R., Hemraz, U.D., Ckless, K., 2016. Cellulose Nanocrystals: a Versatile Nano Platform for Emerging Biomedical Applications. *Expert Opinion on Drug Delivery,* Volume 13(9), pp. 1243–1256

Suryanti, V., Kusumaningsih, T., Safriyani, D., Cahyani, I.S., 2023. Synthesis and Characterization of Cellulose Ethers from Screw Pine (Pandanus tectorius) Leaves Cellulose as Food Additives. *International Journal of Technology*, Volume 14(3), pp. 659–668

Uetani, K., Yano, H., 2011. Nanofibrillation of Wood Pulp Using a High-speed Blender. *Biomacromolecules,* Volume 12(2), pp. 348–353

Väisänen, S., Pönni, R., Hämäläinen, A., Vuorinen, T., 2018. Quantification of Accessible Hydroxyl Groups in Cellulosic Pulps by Dynamic Vapor Sorption with Deuterium Exchange. *Cellulose*, Volume 25(12), pp. 6923–6934

Varshney, S., Mulpuru, V., Mishra, N., Gupta, M.K., 2022. Microwave-irradiated Novel Isolation of Nanocellulose from Waste Rice Husk via Modified Chemo-mechanical Route: Characterization, in-silico Prediction, and its Antibacterial Activity. *Materials Technology*, Volume 37(13), pp. 2608–2622

Wada, M., Okano, T., 2001. Localization of Iα and Iβ Phases in Algal Cellulose Revealed by Acid Treatments. *Cellulose*, Volume 8(3), pp. 183–188

Wyman, C., Decker, S., Himmel, M., Brady, J., Skopec, C., Viikari, L., 2004. Hydrolysis of Cellulose and Hemicellulose. *Polysaccharides: Structural Diversity and Functional Versatility*, Volume 1, pp. 1023–1062

Yuanita, E., Pratama, J.N., Mustafa, J.H., Chalid, M., 2015. Multistage Preparation for Microfibrillated Celluloses Based on Arenga Pinnata "ijuk" fiber. *Procedia Chemistry,* Volume 16, pp. 608–615

Yue, Y., 2011. A Comparative Study of Cellulose I and II Fibers and Nanocrystals. *Louisiana State University and Agricultural and Mechanical College*